Materials Advances

ROYAL SOCIETY OF CHEMISTRY

PAPER

View Article Online
View Journal | View Issue

Cite this: *Mater. Adv.*, 2023, 4, 1089

Dual-responsive microcapsules with tailorable shells from oppositely charged biopolymers for precise pesticide release†

Xiaona Yu, [a] Jie Wang,[ab] Xue Li,[a] Shuaishuai Ma,[a] Wanbin Zhu[a] and Hongliang Wang *[a]

Controlled-release systems are effective in improving the utilization efficiency of pesticides. Here, pH/laccase responsive microcapsules with tunable release performances were prepared by the layer-by-layer deposition of sodium lignosulfonate (SL) and chitosan (CH) for protecting photosensitive avermectin (AVM). First, the homogeneity of AVM was improved by recrystallization for the better investigation of its encapsulation and release performance, and this was confirmed by X-ray diffractometry and Fourier-transform infrared spectroscopy characterization. Subsequently, the microcapsules were prepared *via* a layer-by-layer assembly strategy. It was found that electrostatic interactions rather than chemical reactions were the main driving forces for the formation of the AVM@(CH + SL)*n* microcapsules. AVM@(CH + SL)*n* not only had a high encapsulation efficiency (over 90%), but also exhibited outstanding performance in terms of sustained release and antiphotolysis of AVM. As a result, the 80% AVM release time (t_{80}) of AVM@(CH + SL)5 was 197.24 h, which was much higher than that of the commercial formulation (94.20 h). More importantly, AVM@(CH + SL)*n* was responsive to laccase and pH. The release of AVM from AVM@(CH + SL)5 at an enzyme activity up to 500 U g^{-1} was increased by 181.02%. Under alkaline conditions, the interaction between CH and SL was weakened, which also greatly enhanced the release of AVM. These results confirmed that laccase and the unique alkaline environment in Lepidopteran pests could act as trigger factors for AVM release by AVM@(CH + SL)*n*. Overall, the novel pesticide carrier system prepared in this study can realize the precise release of pesticides as well as the high-value utilization of natural biomass resources.

Received 20th November 2022,
Accepted 24th December 2022

DOI: 10.1039/d2ma01046a

rsc.li/materials-advances

Introduction

Agrochemicals including pesticides provide a reliable guarantee for the stable production of food and other bulk farm-products to meet the demands of a fast-growing population. However, the current pesticide utilization efficiency is rather low, and less than 0.1% of the total dosage is able to reach the targeted sites due to leaching, deposition, photodegradation, hydrolysis, and microbial activity.[1,2] For example, avermectin (AVM) is an important biopesticide that is extensively used in agriculture and animal husbandry. However, the conjugated double bond and macrolide structure of AVM are sensitive to UV irradiation, which results in its short half-life (DT_{50}) under illumination. The DT_{50} of AVM on crop leaves is less than 6 h.[3] As a consequence, indiscriminate and excessive use of agrochemicals is always adopted to achieve the desired efficacy, resulting in high costs and serious environmental issues, such as increasing the resistance of pests and threatening human health.[4]

To overcome this limitation, various pesticide carrier systems on the micro- and nano-scales, such as nanoparticles,[5] nanoemulsions,[6] Pickering systems,[7] and coacervation systems,[8] have been developed, which can continuously release active ingredients over a long period, offering a competent alternative for pest management. These systems usually have the advantages of small volume, large surface area, high loading capacity, superior stability, and dispersibility when compared with their bulky equivalents. However, mainstream methods for preparing these carrier systems involve large amounts of hazardous shell materials, supports, and/or organic solvents, which pose a significant threat to the environment and human health. Besides, current carrier systems can hardly regulate the release behavior of

[a] *Center of Biomass Engineering/College of Agronomy and Biotechnology, China Agricultural University, Beijing, 100193, China. E-mail: Hlwang@cau.edu.cn*
[b] *CAS Key Laboratory of Colloid, Interface and Chemical Thermodynamics, Beijing National Laboratory for Molecular Sciences (BNLMS), CAS Research/Education Center for Excellence in Molecular Sciences, Institute of Chemistry, Chinese Academy of Sciences, Beijing 100190, P. R. China*

† Electronic supplementary information (ESI) available. See DOI: https://doi.org/10.1039/d2ma01046a

active ingredients, leading to a mismatch of drug feeding and demand. Moreover, most of the carrier systems have a single function, and cannot satisfy complex actual application requirements. Therefore, the development of multifunctional pesticide carrier systems, *e.g.*, with anti-photolysis performance and controllable release behavior, using green and inexpensive materials deserves in-depth investigation.

Natural biopolymers, such as lignin,[9] chitosan,[10] and sodium alginate,[11] have attracted increasing attention in preparing drug delivery systems due to their features of low cost, quick regeneration, environmental friendliness, and easy access. Among them, lignin is particularly conspicuous. Lignin is one of the three major components of lignocellulosic biomass, and it is also the only renewable aromatic resource that can be obtained in a large quantity in nature.[12] Over 50 million tons of lignin is generated as a by-product from the pulp and paper industry annually, and more lignin waste is predicted to be produced from biorefinery processes. Lignin holds great potential in the preparation of value-added aromatic chemicals[13,14] and high energy density fuels.[14,15] However, the complicated nature of the biopolymer as well as its disordered degradation products limits its utilization in chemical and fuel production. In recent years, lignin has been frequently used in preparing carrier systems for pesticide delivery due to its characteristics of ultraviolet absorption, oxidation resistance, and amphipathy. In this aspect, alkali lignin is used to prepare micro-nano particles for encapsulating drugs by the anti-solvent method, which is simple to operate but requires large amounts of organic solvents, such as dioxane and tetrahydrofuran, for the dissolution process.[16] Lignosulfonate is another important derivate of lignin and a by-product of paper production from the sulfite pulping process. Compared with other technical lignins, lignosulfonate exhibits excellent water-solubility and polyanion characteristics due to its functional sulfonate groups.[17] Using lignosulfonate as a wall material for preparing carrier systems does not require organic solvents but requires lots of cationic surfactants, such as CTAB or CTAC,[18] which is also not environmentally friendly. More importantly, the shell thickness of current lignin pesticide carrier systems is hard to tune, making the precise delivery of the drug impossible.

Chitosan is a cationic biopolymer derived from the alkaline deacetylation of chitin, one of the most abundant natural polysaccharides.[19] Chitosan contains a large number of highly hydrophilic amino groups,[20] giving the biopolymer a net positive charge favorable for interacting with many negatively charged polymers.[21,22] Therefore, it is possible to construct pesticide carrier systems with a tailored wall thickness through layer-by-layer assembly of lignosulfonate and chitosan. By successfully implementing this strategy, amines in chitosan can interact with sulfonic groups in lignosulfonate *via* electrostatic forces to form a multilayer "eggshell" structure (Scheme 1). Layer-by-layer self-assembly of polymers with opposite charges has been proposed by others. For example, Cheng *et al.*[23] used biopolymers as the shell material for encapsulating red phosphorus and applied it as a flame retardant for epoxy resin. This strategy has also been used for the preparation of pesticide-loaded particles. Wang *et al.*[24] prepared microcapsules loaded with the herbicide picloram using lignin and other biopolymers as the shell material. However, previous investigations only demonstrated the feasibility of encapsulating drugs or loading pesticides by a layer-by-layer assembly strategy, they did not realize the precise regulation of drug release by tuning shell properties. More importantly, previous studies have not explored the response potential of the resulting microcapsules, thereby underestimating their application scope. Targeted drug delivery is an important means to achieve precise drug release, however it puts high requirements on drug delivery systems. Alkaline conditions in the lepidopteran gut and the presence of laccase can be used as

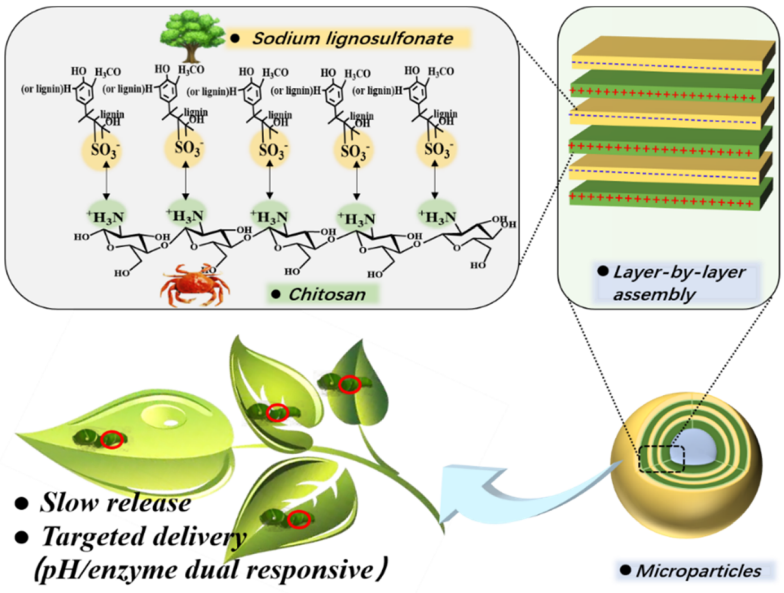

Scheme 1 Scheme of AVM@(CH + SL)*n* formation *via* ionic layer-by-layer (LbL) assembly of chitosan (CH) and lignosulfonate (SL).

triggers to achieve targeted drug delivery.[25] The electrostatic interaction between sodium lignosulfonate and chitosan is affected by pH value, and laccase is a common degradation enzyme usually used for lignin degradation.[25,26] Therefore, it is speculated that the "eggshell" structure formed by lignosulfonate and chitosan provides a possibility for the targeted release of AVM for controlling injurious insects.

In this study, dual-responsive AVM@(CH + SL)*n* microcapsules were prepared by the layer-by-layer (LbL) assembly of chitosan and sodium lignosulfonate on AVM crystals. The recrystallized AVM was obtained by using the anti-solvent method so as to increase the homogeneity of the pesticide raw material. During the LbL assembly process, Fourier Transform infrared spectroscopy (FT-IR), UV-Vis spectroscopy (UV-vis), a Zetasizer Nano-ZS, and confocal laser scanning microscopy (CLSM) were used to verify that chitosan and sodium lignosulfonate had successfully been deposited on the recrystallized AVM. The microstructures of the prepared pesticide carrier system were analyzed using optical microscopy and scanning electron microscopy (SEM). Moreover, the anti-photolysis property, response to pH as well as laccase, and actual insecticidal properties of AVM@(CH + SL)*n* were systematically evaluated, which revealed that the current pesticide carrier system exhibited super performance in pesticide anti-UV protection and precise delivery.

Materials and methods

Chemicals and materials

AVM (powder) was provided by Lier Chemical Co., Ltd, China. Chitosan (CH) with 95% deacetylation and a molecular weight of 50–150 kDa was purchased from Aladdin Reagent Co. Ltd (Shanghai, China). It has a viscosity of 50–100 mPa s and was provided as an off-white powder. Sodium lignosulfonate (SL, with 96% purity, M_w = 534.51) and fluorescein isothiocyanate (FITC) were purchased from Rhawn Co., Ltd, China. A commercial AVM emulsion with 5% active ingredient was purchased from Jinong Crop Protection Ltd (Jiangxi, China). Laccase (2 U mg^{-1}) was obtained from Nanjing Duly Biotechnology Co. Ltd (Nanjing, China). Other chemicals were purchased from Sinopharm Chemical Reagent Co. Ltd (China), and they were all of analytical grade and used as received.

Recrystallization of AVM

1 g of AVM powder was dissolved in 100 mL of anhydrous ethanol under rapid agitation, and then an excess amount of deionized water (about 150 mL) was added *via* a peristaltic pump at a speed of 10 mL min^{-1} under stirring. AVM was precipitated completely after about 2 h and then filtered with organic syringe filters (0.45 μm). Finally, the obtained recrystallized microcrystals were dried at 35 °C and kept in a desiccator for further use. All operations were performed in the dark. The ratio of recrystallized AVM to the original added AVM was calculated as AVM yield to be above 99%.

Deposition of CH/SL multilayers on AVM surfaces

A 0.1 wt% CH aqueous solution was prepared by dissolving CH in a 2% (v/v) acetic acid solution under stirring for 24 h, and the solution pH was adjusted to 4 using HCl and NaOH. SL was dissolved into deionized water to prepare the stock aqueous solution of SL (1 wt%). The recrystallized AVM was dispersed in 5 mL of the CH solution under mechanical stirring for 20 min. After that, the AVM adsorbed with chitosan was separated from the CH solution by centrifugation and dried at 35 °C. Subsequently, the chitosan-coated AVM was immersed in 3 mL of SL aqueous solution under mechanical stirring for 20 min, which was followed by the same separating and drying procedure. The above steps were repeated *n* times to fabricate multilayers containing alternating *n* layers of CH and *n* layers of SL, defined as (CH + SL)*n*.

Evaluation of physicochemical properties of coated AVM and uncoated AVM

An Olympus (CX31, Japan) optical microscope was used for observing the morphology features of raw AVM powder and recrystallized AVM. The scanning electron microscopy (SEM) micrographs of coated AVM and uncoated AVM were recorded with a JSM-7800 scanning electron microscope. Samples were metal sprayed in advance. X-ray diffraction (XRD) patterns of the samples were obtained by using a diffractometer (Ultima IV, Japan) with Cu Kα radiation to characterize the structure of the prepared nanoparticles. The diffraction patterns were recorded in the 2θ range of 10–80° with a scanning speed of 10° min^{-1}. A Zeta-sizer Nano ZS (Malvern Instruments, Malvern, UK) was used to measure the zeta potential data. Before the test, particles were dispersed in water to form a 0.5 wt% suspension. Each sample was tested in triplicate. AVM@(CH + SL)*n* and the precursors (AVM, CH, and SL) were also subjected to FT-IR spectral analysis using a TENSOR II Fourier transform spectrophotometer (Bruker, Germany). The wavenumber range was set from 400 to 4000 cm^{-1} and the resolution of the spectra was 4 cm^{-1}. The core–shell structure of AVM@(CH + SL)*n* was observed using Confocal Laser Scanning Microscopy (CLSM). CH was labeled with fluorescein isothiocyanate (FITC) to visualize the particles. Under alkaline conditions, the isothiocyanate of FITC could covalently bind with the primary amino group of CH, providing the CH molecules with an obvious fluorescence effect.[27] The coated AVM microcrystals were analyzed using a confocal scanning system equipped with a 40 × objective (ZEISS/LSM 880, Germany), and the excitation wavelength was set to 488 nm. Particle dispersion samples were diluted to a concentration of 0.5% (w/v). UV absorption spectra of SL, CH, AVM, and AVM@(CH + SL)*n* dispersions were recorded in the range of 200–600 nm by a UV spectrophotometer (Shimadzu UV-2550, Japan).

Measurements of AVM loading (AL) and encapsulation efficiency (EE)

10 mg of AVM@(CH + SL)*n* or 1 mL of commercial AVM emulsion was dissolved in 20 mL of ethanol/water (80/20, v/v) and placed in an ultrasonic bath for 30 min. The resulting AVM extracts were filtrated by organic syringe filters (0.45 μm), and

the concentration of loaded AVM was analyzed using high performance liquid chromatography (HPLC, Waters, USA) with isocratic elution of methanol–water (90/10, v/v) as the mobile phase. 10 μL of the analyte was injected into the HPLC system and separated at a flow rate of 1 mL min^{-1} under a detection wavelength of 245 nm. The standard curves for determining the AVM content are shown in Fig. S1 (ESI†). The AVM loading and encapsulation efficiency were calculated according to the following equations, respectively:

$$\mathrm{AL}(\%) = \left(\frac{\text{Weight of AVM loaded}}{\text{Weight of AVM@(CH + SL)}n}\right) \times 100$$

$$\mathrm{EE}(\%) = \left(\frac{AVM\ loading}{\text{Initial amount of AVM}}\right) \times 100$$

Sustained-release behavior of AVM@(CH + SL)*n*

AVM release from the microcapsules was evaluated through a dynamic dialysis method. 20 mg of AVM@(CH + SL)*n* or 0.5 mL of commercial AVM was suspended in 20 mL of water and then transferred into a dialysis bag (MwCO = 1000 Da). The dialysis bag was submerged into 170 mL of ethanol/water (80/20, v/v) in a glass bottle and then placed in a shaking incubator with an oscillation rate of 200 rpm at a constant 25 °C. At certain intervals, 1 mL of solution outside the dialysis bag was taken out to test the AVM concentration using HPLC, and, simultaneously, the same volume of fresh ethanol/water solution was added to keep the volume constant. The effects of enzyme and pH on the release profiles of the AVM from AVM@(CH + SL)*n* were examined. The standard procedures for measuring the release profiles are described in the ESI.†

Photostability of AVM@(CH + SL)*n*

To evaluate the light stability of the samples, AVM@(CH + SL) samples coated with 0, 1, 3, and 5 layers together with commercial the AVM emulsion (as control) were dispersed in deionized water. The above suspensions were poured into 4.0 cm diameter glass Petri dishes and dried into thin films in the dark at room temperature. Then, these films were exposed to UV light (40 W, 340 nm) at a distance of 30 cm for 0, 3, 6, 12, 24, 36, 48, 60, and 96 h at room temperature. The remaining content of AVM in each film after UV irradiation was extracted by 20 mL of ethanol through ultrasonication, which was then filtered with a 0.45 μm membrane filter before being detected by HPLC. Each treatment was repeated three times.

Insecticidal activity of AVM@(CH + SL)*n*

The insecticidal activities of AVM@(CH + SL)*n* microcapsules against *P. xylostella* larvae (provided by Beijing Yimeimiao Technology Co., Ltd) were determined by a regular sampling feeding method.[28] AVM@(CH + SL)*n* and commercial AVM emulsions were directly dispersed in 0.1 wt% Triton X-100 aqueous solution to achieve AVM concentrations of 5.0, 2.0, 1.0, 0.4, and 0.2 mg L^{-1}, respectively. These dispersions were then sprayed on *B. oleracea* that had not been treated with pesticides. *B. oleracea* sprayed with blank CH + SL dispersions was used as a control. The sprayed leaves (size: 5.5 × 5.5 cm^2) were collected at certain points (0, 3, 7, and 15 days), and placed on wet filter paper in Petri dishes (one leaf disc per plant). Ten third-instar larvae were tested for each concentration, and each treatment was replicated three times. The Petri dishes were placed in an incubator at 26–27 °C and 60% humidity. Finally, the mortality of *P. xylostella* larvae was recorded after 3 days. The criterion for death was: touched by the brush, without bending.

To further examine the insecticidal activity, AVM@(CH + SL)*n* dispersions with an effective AVM concentration of 5 mg L^{-1} before and after UV irradiation were studied using a leaf-dipping assay.[5] The collected leaves of *B. oleracea* (size: 5.5 × 5.5 cm^2) were immersed into each treatment dispersion for 1 min. The UV irradiation (40 W lamp, 340 nm) was conducted continuously for 10 h at a distance of 35 cm. Subsequently, the treated leaves were placed into Petri dishes lined with filter paper, and ten third-instar larvae were then placed in each dish. The mortality of the tested insects was investigated after 3 days.

Results and discussion

AVM recrystallization

The release behaviors of active ingredients (drugs) in carrier systems are usually determined by internal factors including shell material properties, and drug size, shape,[29] and solubility, as well as external conditions such as solvent, temperature, pH, ionic strength, *etc.*[29,30] The commercial AVM microcrystals have rough surfaces, irregular shapes, and varying sizes, as shown in Fig. 1(a) and (b), which adversely affect the further assembly of shell materials on them. Particularly, AVM crystals with different sizes would dissolve at different rates due to the fact that they have different surface–volume ratios, resulting in an obvious influence on drug release behavior. The large heterogeneity of the raw AVM material is disadvantageous to the subsequent study of the release behavior of AVM from carrier systems, therefore it is necessary to implement a recrystallization process to improve the homogeneity of AVM crystals.

AVM presenting as light yellow or white crystalline powder is stable under normal conditions.[28] It is almost completely insoluble in water (10 μg L^{-1}) and has a solubility of 20 g L^{-1} in ethanol.[31] Therefore, in this study, the anti-solvent method was used to recrystallize AVM. The morphology of the recrystallized AVM is shown in Fig. 1(c) and (d). Compared with the raw AVM, the recrystallized AVM microcrystals are present in long columnar shapes with lengths of 25–50 μm. AVM after recrystallization shows more regular shapes and uniform sizes, which are conducive to the subsequent investigation of the LbL assembly process and drug release behavior. Except for the changes of morphology, the recrystallization process shows no effect on the chemical structure of AVM, as can be seen from Fig. 1(e) and (f), indicating that recrystallized AVM should retain its insecticidal activity.

Encapsulation of AVM *via* the layer-by-layer assembly of CH and SL

AVM encapsulated by different layers of SL and CH was prepared *via* the LbL assembly strategy. The chemical structures of SL, CH,

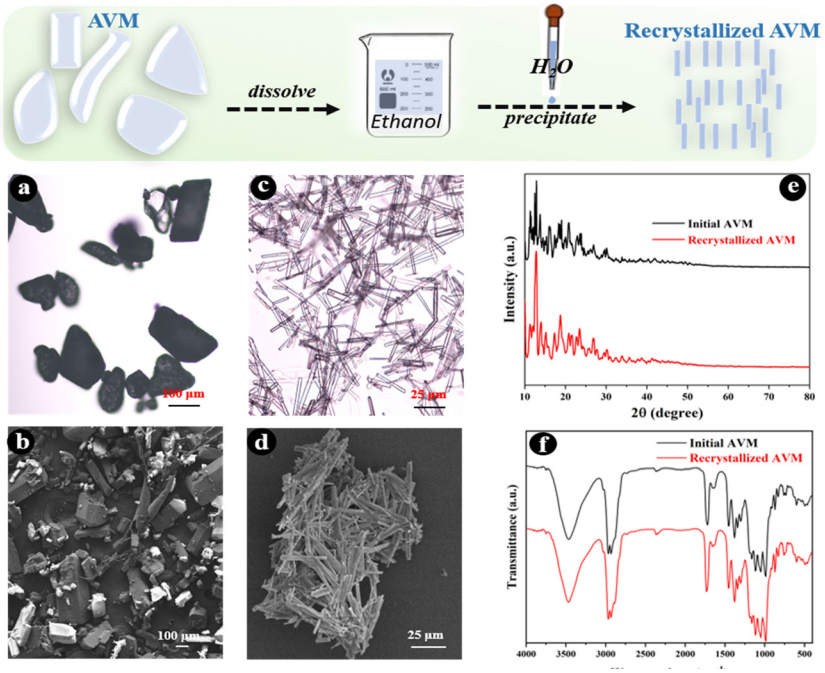

Fig. 1 Optical micrographs (a) and (c), SEM micrographs (b) and (d), X-ray diffraction patterns (e), and FT-IR spectra (f) of AVM microcrystals before and after recrystallization.

and AVM@(CH + SL)*n* were analyzed using FT-IR spectroscopy and the results are shown in Fig. 2(a). For SL, the absorption bands at 1512 and 1043 cm^{-1} corresponded to the C_9 aromatic skeletal vibration and the stretching vibration of S═O, respectively.[24] The absorption peaks of CH at 3600–3200 cm^{-1} originate from the stretching vibration of the O–H group combined with the N–H group, and the peaks at 1654 and 1596 cm^{-1} are responsible for the amide I and II bands, respectively.[23,24] Regarding the CH + SL shell, the original characteristic absorptions of the S═O group at 1043 cm^{-1} for SL and the amide I and II at 1654 and 1596 cm^{-1} for CH almost completely disappear, and new absorption peaks appear around 1569 cm^{-1}, which suggests a strong electrostatic interaction between the positively charged amino groups ($-NH^{3+}$) and the negatively charged sulfuric acid ions ($-SO^{3-}$), resulting in a redshift of absorption peaks. The above results indicate that CH and SL were successfully deposited on the surface of AVM *via* electrostatic interaction rather than by chemical reaction.

Detailed information about the surface charge density of particles was obtained from zeta potential data. The zeta potential value depends on the net charge and properties of the functional groups located on the surface of the microcapsules.[32] The alternative deposition of CH and SL on AVM crystals was monitored by zeta-potential measurement, as shown in Fig. 2(b). The surface of the uncoated AVM was negatively charged with a potential of −25.0 mV, enabling CH adsorption as the first layer. Subsequently,

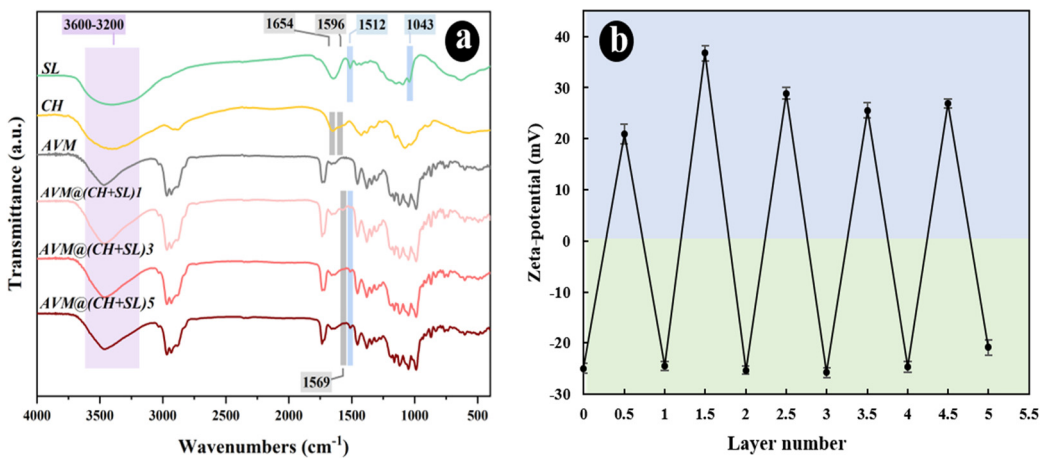

Fig. 2 The FT-IR spectra (a) and zeta potential (b) of SL, CH, and AVM@(CH + SL)*n*.

the deposition of SL on CH coated AVM crystals reversed the zeta potential to 20.9 mV. The surface-modified AVM particles were prevented from aggregating due to the ionic and/or steric interactions of the thin coatings, and therefore they were stable in the aqueous system. Alternating and regular reversals of the zeta potential were observed with the further deposition of oppositely charged CH and SL on the particles. The obvious alternating zeta potentials imply the successful formation of AVM@(CH + SL)*n via* layer-by-layer assembly.

Fig. 3 shows SEM micrographs of AVM and AVM@(CH + SL)*n*. The uncoated AVM microcrystals exhibited a smooth surface, while after being coated by one layer of CH + SL, the shape as well as the surface morphology of the particles was obviously different (Fig. 3(b), (f) and (j)). The size of the AVM particles decreased during LbL assembly, because the rod-like crystals were broken under the condition of agitation. Additionally, the crystal surface turned rough with partial exposure of AVM, indicating that the shell material did not completely cover the AVM core material after coating one layer. Whereas, crystals encapsulated with five layers of CH + SL had a much rougher surface than those with one layer, and the AVM was completely covered by the shell materials. CLSM was employed to verify the coating of CH on AVM. As can be found in Fig. 3(l), a homogeneous green fluorescence intensity was observed on the particles, which originated from FITC on CH. This result indicates that CH + SL completely and uniformly wraps AVM after coating with 5 layers. The fluorescence intensity present in Fig. 3(j) is weak because the content of wall material was relatively low after coating one layer.

Table 1 lists the loading and encapsulation efficiency of AVM in microcapsules with different coating layers. The loading of AVM after coating one layer reached 97.72% due to the low content of wall material in the microcapsules. With the increase of coating layers, the loading of AVM gradually decreased and the encapsulation efficiency was also reduced because of repeated centrifugal cleaning operations that inevitably led to AVM loss. Nevertheless, both AVM loading and encapsulation efficiency were maintained at a high level (over 90%) after coating five layers. The above results further demonstrated that the preparation of AVM microcapsules with superior drug loading properties and tailored wall thickness through the LbL assembly strategy was successful.

Table 1 AVM loading and encapsulation efficiency of AVM@(CH + SL)*n*

Microcapsules	AVM Loading (%)	Encapsulation efficiency (%)
AVM@(CH + SL)1	97.72	98.32
AVM@(CH + SL)3	93.22	92.12
AVM@(CH + SL)5	91.34	90.11

Photostability of AVM@(CH + SL)*n*

The LbL assembly process of CH + SL on AVM can also be monitored using UV-vis absorption spectroscopy. Fig. 4(a) shows the UV-visible absorption spectra of the different materials. Pristine CH and AVM have almost no absorption peaks. SL shows an obvious absorption peak at 280 nm, which was ascribed to the UV absorption of aromatic rings.[33] When SL was deposited on the AVM surface, the UV absorption capacity of AVM@(CH + SL)*n* was increased. The more layers coated, the stronger the UV absorption ability. The slight change of UV absorption peak position was related to the interaction between SL and CH. These results indicate that CH + SL is an effective anti-UV shell that may have the ability to protect AVM from photolysis.

To verify the above speculation, the direct photolysis of AVM@(CH + SL)*n* was carried out under UV lamp irradiation with wavelength ranging from 280 to 365 nm, which is relatively similar to the UV range of sunlight (290–400 nm). During photolysis, all samples were used in a dried form to test the direct effect

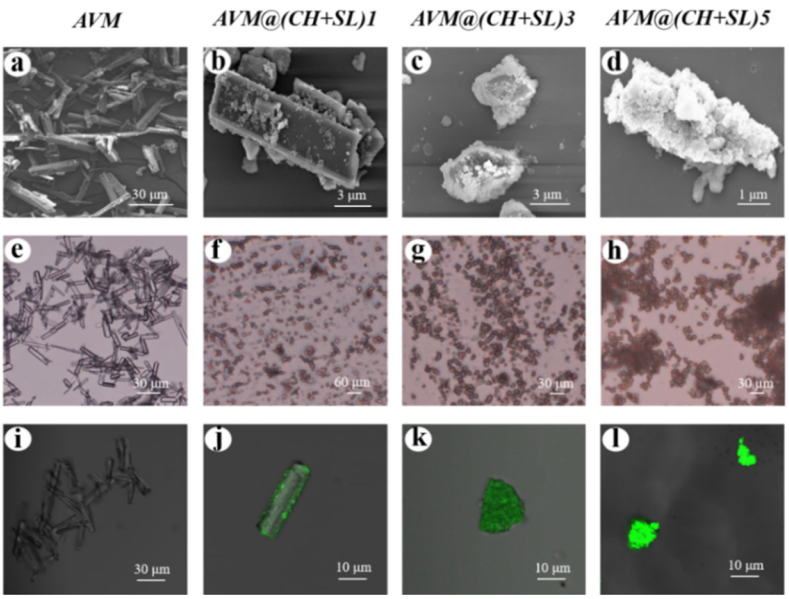

Fig. 3 SEM micrographs (a)–(d), optical micrographs (e)–(h), and CLSM images (i)–(l) of AVM and AVM@(CH + SL)*n*.

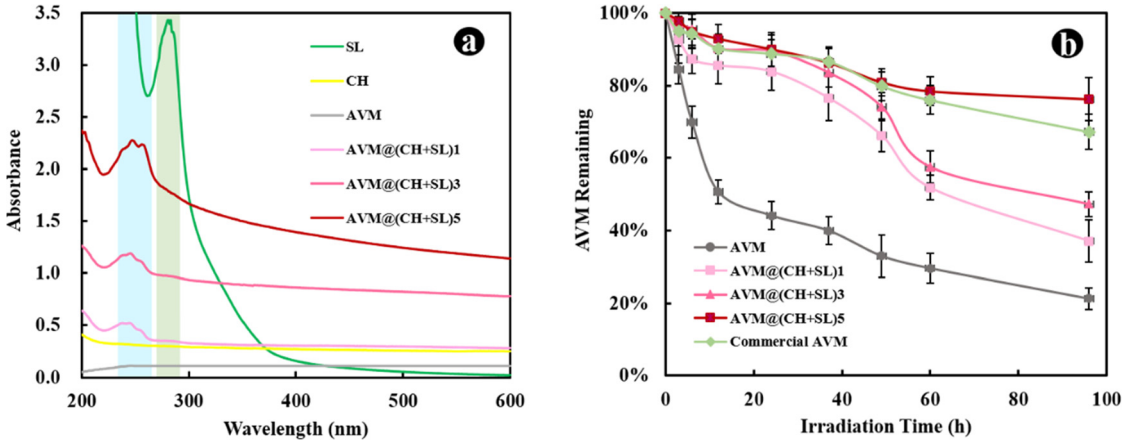

Fig. 4 (a) UV-vis absorption spectra of CH, SL, AVM, and AVM@(CH + SL)*n*. (b) Percentages of AVM remaining in microcapsules with 1, 3, and 5 layers after being exposed to UV light in comparison to the uncoated AVM and commercial AVM emulsion (error bars represent the standard deviation of three replicates).

of UV irradiation on uncoated AVM and AVM@(CH + SL)*n*. As depicted in Fig. 4(b), the uncoated AVM undergoes a rapid photodegradation, while AVM protected by (CH + SL)*n* shells is relatively stable. After UV exposure for 96 h, the remaining amount of AVM (76.29%) in AVM@(CH + SL)5 was approximately 4 times that of the uncoated AVM (21.28%). Furthermore, the stability of AVM in the microcapsules increases as the layer number increases. AVM@(CH + SL)5 shows a better protective effect on AVM than the commercial AVM emulsion, which uses lots of organic solvent and surfactants to stabilize AVM. The excellent anti-UV property of the microcapsules is mainly ascribed to the uniform deposition of SL on AVM. Besides, CH is able to slightly absorb UV-A and UV-B radiation, and can also scatter UV light.[34] All these results suggest that the prepared carrier system has the desired performance for protecting photosensitive pesticides.

AVM release behavior of AVM@(CH + SL)*n*

The AVM release behavior of the prepared microcapsules was subsequently investigated using the dynamic dialysis method. The released AVM from the sample solutions was collected at different time intervals and quantified by HPLC. As shown in Fig. 5, AVM release can be divided into two stages: a first burst release stage and a second slow-release stage. This result is due to the fact that during the initial release period, the concentration gradient between the donor medium and the recipient is high, coupled with the quick dissolution of a small number of incompletely wrapped AVM particles, resulting in a burst release of AVM to the solution.[24,35] In the slow-release stage, the concentration gradient of AVM becomes small, and AVM encapsulated inside the carrier system experiences greater resistance to migrating to the outside. The initial burst release is a big problem for controlled release systems, since the acute liberation of a high amount of drug not only causes drug waste but also increases the risk of pesticide damage to crops and the environment. The 80% AVM release time (t_{80}) was 105.82 h for AVM@(CH + SL)1, 152.21 h for AVM@(CH + SL)3, 197.24 h for AVM@(CH + SL)5, and 94.20 h for the commercial AVM emulsion. As expected, the AVM release time could be well tuned by adjusting the number of coating layers on the microcapsules, and the initial AVM "burst effect" could also be relieved after encapsulation.

Next, the mechanism of AVM release from AVM@(CH + SL)*n* was investigated. AVM release from microcapsules mainly involves two processes: (i) bulk solvents diffuse across the wall of the microcapsules to dissolve drug microcrystals, and (ii) the dissolved AVM molecules diffuse out of the microcapsules.[36] Accordingly, there are two main factors that determine the drug release rate. One is the drug concentration differential between the inside and outside of the microcapsule. The other is the permeability of the wall material. During the early release stage, core materials (AVM crystals) were not completely dissolved by solvents, and thus AVM concentration within the microcapsules was very high and stable, making the concentration differential unchanging. During this period, the AVM release

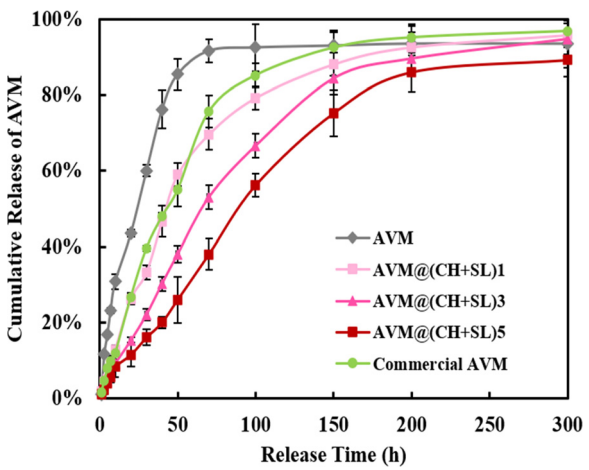

Fig. 5 Release profiles of AVM from AVM@(CH + SL)*n* with 1, 3, and 5 layers in comparison to the uncoated AVM and commercial AVM emulsion (error bars represent the standard deviation of three replicates).

rate was mainly determined by the permeability of the microcapsule wall. Therefore, increasing the microcapsule wall thickness by multilayer deposition would decrease the release rate of AVM.[37] With the total dissolution of the drug and the collapse of wall materials, the concentration differential gradually becomes the decisive factor in the later stage.

Furthermore, the kinetics of AVM release from AVM@(CH + SL)*n* were studied, and data were fitted by different models, as listed in Table S1 (ESI†).[38] Fig. 6 shows a regression analysis of AVM release from different systems. Various models were fitted and evaluated by their regression factors (R_2) to probe AVM release kinetics,[35] and the R_2 values are listed in Table S2 (ESI†). Obviously, the first-order release model was the most suitable one for explaining the AVM release behavior from AVM@(CH + SL)*n*, implying that AVM release was mainly related to the content of AVM in the microcapsules, and indicating that the release behavior of the carrier system was largely governed by the thickness of the wall.[39] For a deeper understanding of the relationship between the number of deposition layers and AVM release rate, t_{80s} values of different microcapsules were exponentially fitted using the number of deposition layers (Fig. 6(f)). The fitting coefficient (R^2) was above 0.995, indicating that the fitting equation has a high accuracy. Therefore, it is possible to precisely control the release rate of the drug by controlling the number of wall layers of the microcapsules *via* a LbL assembly strategy.

Dual-response of AVM@(CH + SL)*n* to laccase and pH

The basic idea of controlled release is to effectively combine wall materials and active ingredients through specific methods, and ensures that the effective concentration of the active ingredient is maintained at a relatively stable level in the corresponding system. Therefore, the active ingredient can be diffused into the surrounding environment at an optimal release rate within a certain period of time.[40] Though remarkable achievements have been made, it is worth putting in sustained efforts in this area to make the following improvements: (1) simplify the preparation processes of carrier systems, and reduce the preparation costs. The controlled-release system AVM@(CH + SL)*n* prepared in the current study does not require complex processes, and the preparation conditions, as well as equipment, are quite normal, which enables it to be used at a low cost and on a large scale. (2) Develop carrier systems to achieve

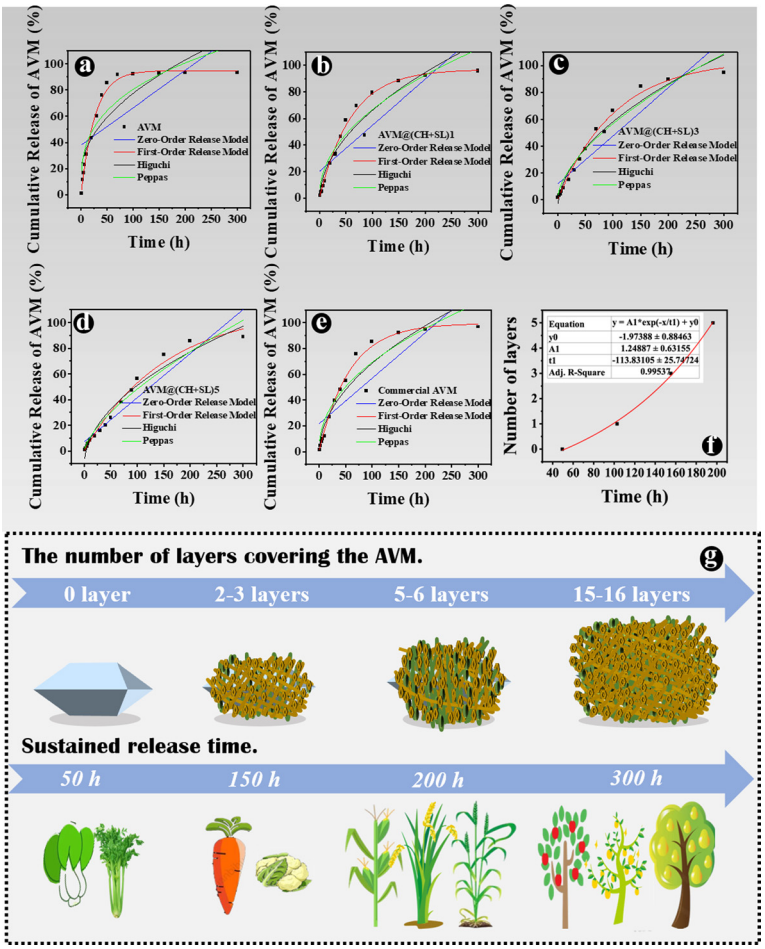

Fig. 6 Fitted regression lines for AVM released from uncoated AVM (a), AVM@(CH + SL)*n* (b)–(d) and the commercial AVM emulsion (e). Fitted curve of the layer number *n* in AVM@(CH + SL)*n* microcapsules *versus* the time at 80% AVM release (f). Schematic diagram of the layer number *n* covering AVM *versus* release time and application scenarios (g).

improvement from sustained release to controlled release. Most of the current pesticide controlled-release systems can only realize sustained release rather than controlled release. The irregular and uncontrollable release of active substances will certainly evolve to accurate, quantitative, and controlled release, that is, releasing a specific amount of active ingredients at the appropriate time and location according to the actual regulatory needs. On the basis of results from Fig. 6(f), AVM release from AVM@(CH + SL)*n* can be finely tuned by controlling the thickness of the microcapsule wall. This can provide a customized pesticide carrier system for different crops and different application scenarios (Fig. 6(g)), thereby improving drug utilization efficiency and reducing the harm of drugs to the environment. (3) Screen and develop green materials for use as microcapsule wall structure, conforming to the concept of green manufacturing and sustainable development. The wall materials of chitosan and lignin used in this study are from marine and terrestrial biomass, respectively.[41] They are rich in sources, and are safe and friendly to the environment and organisms.[41,42] (4) Develop carrier systems with intelligent release performances, which means these systems could release drugs in response to specific stimulations including pH,[43] temperature, light,[44] humidity, and enzymes.[45] Therefore, we next explored the intelligent response behavior of AVM@(CH + SL)*n*.

The development of drug delivery systems with responsive mechanisms is an important strategy to achieve precise drug release. The shell of AVM@(CH + SL)*n* is a lignin derivative that can be degraded by laccase, a lignin-degrading enzyme in the digestive tract of lepidopterans.[25] AVM@(CH + SL)5 was used as an example to test the release properties regulated by laccase. The results showed that laccase could indeed accelerate the release of the AVM from the microcapsules (Fig. 7(a)). At 40 h, the final release of AVM increased by 45.23% in 50 U g^{-1} laccase solution, 100.19% in 100 U g^{-1} laccase solution, and 181.02% when the enzyme activity reached 500 U g^{-1}. The release mechanism mainly involves the gradual decomposition of laccase to sodium lignosulfonate. With the prolongation of time, it is speculated that the outer wall of AVM@(CH + SL)*n* becomes thin or even perforated under the action of laccase,[25] leading to the rapid release of AVM.

Alkaline conditions in the intestinal tract of lepidopterans are often used as a trigger to achieve targeted drug delivery. Therefore, the response of the microcapsules to pH was investigated. As displayed in Fig. 7(b), alkaline conditions significantly increased the release of AVM from AVM@(CH + SL)5 over 40 h compared with neutral and weakly acidic environments. The reason is that CH is a weak electrolyte, and when the pH of the system is $\geq$6.5, the insufficient charge density of CH molecular chains leads to an unstable assembly. Moreover, the sulfonic acid groups on the SL molecule can be completely ionized under alkaline conditions,[26] which resulted in the dissolution of SL. Therefore, the peak at 280 nm, which represents the UV absorption of SL in Fig. 7(c), increased in intensity. In short, the microenvironment in the lepidopterans can promote the rapid release of AVM in AVM@(CH + SL)*n*, so as to achieve the purpose of targeted insecticide delivery (Fig. 7(d)).

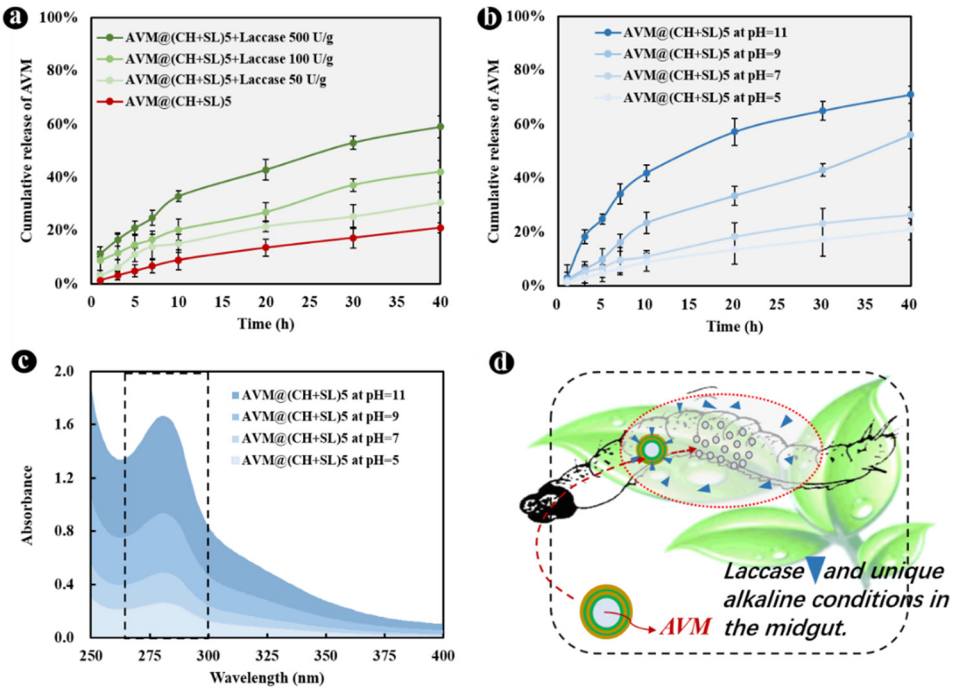

Fig. 7 Effects of laccase (a) and pH (b) on the release performance of AVM from AVM@(CH + SL)5; (c) UV-spectra of supernatants from AVM@(CH + SL)5 at different pH values; (d) schematic of the targeted delivery of AVM@(CH + SL)*n* in the digestive tract of pests (error bars represent the standard deviation of three replicates).

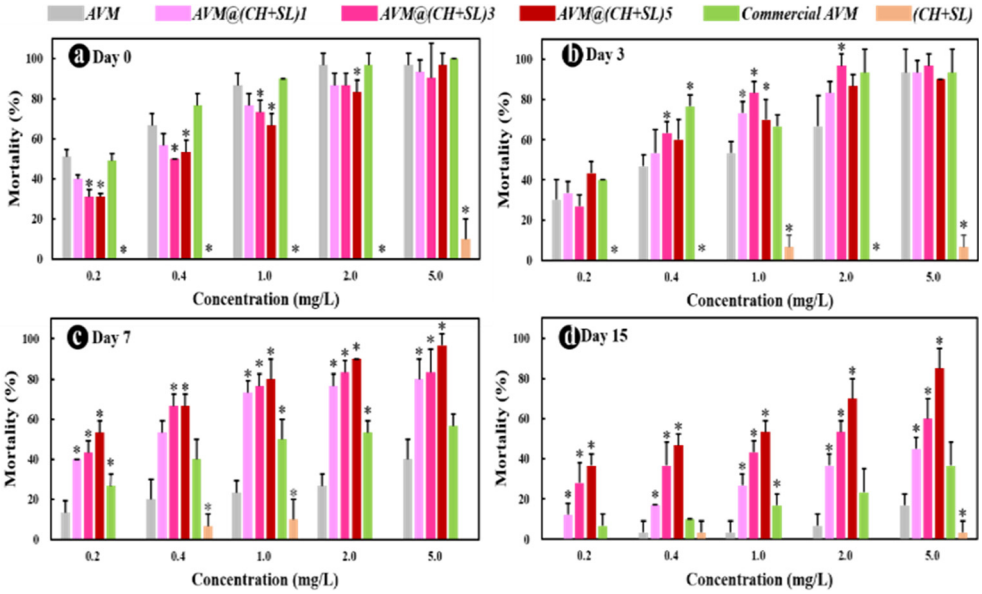

Fig. 8 Mortality of different concentrations of pure AVM, AVM@(CH + SL)*n*, and commercial AVM against *P. xylostella* larvae. Statistically significant differences are indicated by $^*P < 0.05$ as compared with AVM.

Insecticidal activity

Finally, to investigate the practical performance of AVM@(CH + SL)*n* in agricultural applications for controlling harmful insects, third-instar *P. xylostella* larvae were chosen as model insects to evaluate the insecticidal activity of the microcapsules. The uncoated AVM, commercial AVM emulsion, and blank (CH + SL) were used as controls. As shown in Fig. 8, blank (CH + SL) showed negligible toxicity towards *P. xylostella* larvae. In contrast, the mortality rates of uncoated AVM, the commercial AVM emulsion, and AVM@(CH + SL)*n* towards *P. xylostella* larvae were found to be dose-dependent. Under the condition of a high AVM concentration, the insect mortality reached up to 100% at the early stage, and the mechanism of the killing was that AVM blocked the synaptic transmission from the internuncial neurons to the motor nerve cells.[5,46] Among the controls, there was no significant difference between the commercial AVM emulsion and uncoated AVM in killing *P. xylostella* larvae on day 0. As time went on, the mortality caused by both insecticides decreased rapidly, and the commercial AVM emulsion performed better than raw AVM. However, the commercial AVM formulation was still unsatisfactory with a mortality of only 36.67% at 5.0 mg L^{-1} dosage after 15 days of spraying. In comparison, the insecticidal performance of AVM@(CH + SL)*n* remained at a high level after 15 days, and AVM@(CH + SL)5 with a concentration of 5 mg L^{-1} could kill 80% of the pest. However, the low insecticidal activity of AVM@(CH + SL)5 at the early stage was due to the slow release of

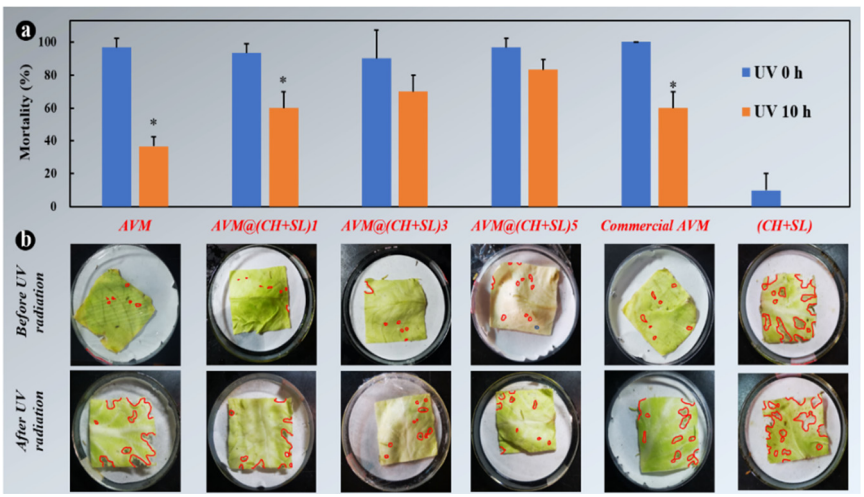

Fig. 9 (a) Toxicity of AVM, AVM@(CH + SL)*n*, commercial AVM, and CH + SL with an effective concentration of 5 mg AVM towards *P. xylostella* larvae. Statistically significant differences are indicated by $^*P < 0.05$ as compared with each treatment without UV irradiation. (b) Photographs of B. oleracea leaves treated with AVM, AVM@(CH + SL)*n*, and commercial AVM before and after UV radiation after feeding *P. xylostella* larvae for 3 days.

the drug due to the multilayers of the wall. Table S3 (ESI†) lists the insecticidal efficacy obtained *via* probability analysis. The median lethal concentration (LC_{50}) values on days 7 and 15 evidenced that the toxicity of AVM@(CH + SL)*n* towards *P. xylostella* larvae was over 10 times that of pure AVM and commercial AVM (Table S3, ESI†). This result indicates that AVM@(CH + SL)*n* prepared by a layer-by-layer assembly strategy can effectively improve AVM use efficiency.

The toxicities of these samples before and after UV irradiation were also investigated and the results are shown in Fig. 9(a). After 10 h of irradiation (40 W UV lamp), the mortality of pure AVM decreased to 36.67%, whereas that of AVM@(CH + SL)5 remained at the high level of 83.33%. There is no significant difference in the toxicity of CH + SL towards pests before and after irradiation. This treatment is almost completely non-toxic, because lignin and chitosan are natural organic polymer materials with good biocompatibility.[7,22] From Fig. 9(b), it can be seen that the leaves treated by AVM and commercial AVM were eaten to a greater extent after irradiation, while the leaves of AVM@(CH + SL)*n* are more complete, indicating that the shell material (CH + SL) can effectively shield the UV light and thus protect AVM from deactivation. This result is consistent with that deduced from Fig. 4. Therefore, AVM@(CH + SL)*n* provides a promising option for pest control in actual applications.

Conclusions

In summary, recrystallized AVM microcrystals were successfully encapsulated by a layer-by-layer (LbL) assembly method using oppositely charged chitosan (CH) and lignin (SL) as wall materials. This method has the advantages of simple operation, low cost, and environmental friendliness. The wall thickness and physicochemical properties of the encapsulated drug could be well tuned by controlling the LbL process. Besides high loading capacity (91.34%) and encapsulation efficiency (90.11%), AVM@(CH + SL)*n* exhibited outstanding long-acting and sustained drug release performance. Moreover, AVM@(CH + SL)*n* microcapsules could effectively protect AVM against photodegradation, avoiding excessive consumption of pesticides. Both the release rate and photodegradation of AVM from AVM@(CH + SL)*n* microcapsules decreased as the layer numbers of CH + SL increased. More importantly, laccase and alkaline conditions could stimulate AVM release, which means that AVM could be released precisely from AVM@(CH + SL)*n* on demand. Bioassay experiments indicated that AVM@(CH + SL)*n* exhibited desirable toxicity towards *P. xylostella* larvae, and had longer activity than the commercial AVM emulsion. Therefore, this innovative strategy not only extends the high-value applications of abundant biomass resources but also provides an economical and environmentally friendly way to improve pesticide use efficiency.

Author contributions

Xiaona Yu: investigation, data curation, formal analysis, writing – original draft preparation. Jie Wang: methodology, formal analysis. Xue Li: methodology, conceptualization, supervision, writing – review & editing. Shuaishuai Ma: supervision, writing – review & editing. Wanbin Zhu: conceptualization. Hongliang Wang: conceptualization; resources; funding acquisition; supervision; writing – review & editing.

Conflicts of interest

There are no conflicts to declare.

Acknowledgements

This work was supported by the National Key R&D Program of China (2021YFA0716700), the National Natural Science Foundation of China (22278422), the 2115 Talent Development Program of China Agricultural University Fund (1011-00109018), and Beijing Innovation Team of the Modern Agricultural Research System (BAIC08-2022). We are also very grateful for the helpful input from the Editor and anonymous reviewers.

Notes and references

1 S. Kumar, G. Bhanjana, A. Sharma, M. C. Sidhu and N. Dilbaghi, *Carbohydr. Polym.*, 2014, **101**, 1061–1067.
2 G. Tang, Y. Tian, J. Niu, J. Tang, J. Yang, Y. Gao, X. Chen, X. Li, H. Wang and Y. Cao, *Green Chem.*, 2021, **23**, 2531–2540.
3 Z. Zhou, Y. Gao, X. Chen, Y. Li, Y. Tian, H. Wang, X. Li, X. Yu and Y. Cao, *ACS Appl. Mater. Interfaces*, 2021, **13**, 39066–39075.
4 R. L. Hough, *Nat. Geosci.*, 2021, **14**, 183–184.
5 M. Zhao, P. Li, H. Zhou, L. Hao, H. Chen and X. Zhou, *Chem. Eng. J.*, 2022, **435**, 134861.
6 Z. Du, C. Wang, X. Tai, G. Wang and X. Liu, *ACS Sustainable Chem. Eng.*, 2016, **4**, 983–991.
7 X. Yu, S. Chen, W. Wang, T. Deng and H. Wang, *J. Cleaner Prod.*, 2022, **339**, 130769.
8 J. Wang, Y. Fan, H. Wang, J. Yin, W. Tan, X. Li, Y. Shen and Y. Wang, *Chem. Eng. J.*, 2022, **430**, 132920.
9 B. L. Tardy, J. J. Richardson, J. Guo, J. Lehtonen, M. Ago and O. J. Rojas, *Green Chem.*, 2018, **20**, 1335–1344.
10 S. Bi, D. Qin, S. Yuan, X. Cheng and X. Chen, *Green Chem.*, 2021, **23**, 9318–9333.
11 E. Lengert, M. Saveleva, A. Abalymov, V. Atkin, P. C. Wuytens, R. Kamyshinsky, A. L. Vasiliev, D. A. Gorin, G. B. Sukhorukov, A. G. Skirtach and B. Parakhonskiy, *ACS Appl. Mater. Interfaces*, 2017, **9**, 21949–21958.
12 M. H. Tran, D.-P. Phan and E. Y. Lee, *Green Chem.*, 2021, **23**, 4633–4646.
13 H. Wang, Y. Duan, Q. Zhang and B. Yang, *ChemSusChem*, 2018, **11**, 2562–2568.
14 S. Chen, Q. Lu, W. Han, P. Yan, H. Wang and W. Zhu, *Fuel*, 2021, **283**, 119333.
15 H. Wang, H. Wang, E. Kuhn, M. P. Tucker and B. Yang, *ChemSusChem*, 2018, **11**, 285–291.

16 P. Figueiredo, M. H. Lahtinen, M. B. Agustin, D. M. Carvalho, S.-P. Hirvonen, P. A. Penttila and K. S. Mikkonen, *ChemSusChem*, 2021, **14**, 4718–4730.
17 F. Zhang, Y. Li, H. Cai, Q. Liu and G. Tong, *Carbohydr. Polym.*, 2020, **241**, 116253.
18 Q. Tang, M. Zhou, Y. Li, X. Qiu and D. Yang, *ACS Sustainable Chem. Eng.*, 2018, **6**, 1379–1386.
19 G. Maleki, E. J. Woltering and M. R. Mozafari, *Trends Food Sci. Technol.*, 2022, **120**, 88–99.
20 K. Crouvisier-Urion, F. R. d S. Farias, S. Arunatata, D. Griffin, M. Gerometta, J. R. Rocca-Smith, G. Weber, N. Sok and T. Karbowiak, *Green Chem.*, 2019, **21**, 4633–4641.
21 H. Qi, G. Pan, X. Shi and Z. Sun, *Chem. Eng. J.*, 2022, **434**, 134675.
22 M. Keshvardoostchokami, M. Majidi, A. Zamani and B. Liu, *Carbohydr. Polym.*, 2021, **273**, 118625.
23 C. Cheng, J. Yan, Y. Lu, W. Ma, C. Li and S. Du, *Thermochim. Acta*, 2021, **700**, 178931.
24 X. Wang and J. Zhao, *J. Agric. Food Chem.*, 2013, **61**, 3789–3796.
25 D. Zhang, J. Du, R. Wang, J. Luo, T. Jing, B. Li, W. Mu, F. Liu and Y. Hou, *Adv. Funct. Mater.*, 2021, **31**, 2102027.
26 K. Luo, J. Yin, Z. Song, L. Cui, B. Cao and X. Chen, *Biomacromolecules*, 2008, **9**, 2653–2661.
27 M. Huang, E. Khor and L. Y. Lim, *Pharm. Res.*, 2004, **21**, 344–353.
28 Y. Liang, Y. Gao, W. Wang, H. Dong, R. Tang, J. Yang, J. Niu, Z. Zhou, N. Jiang and Y. Cao, *J. Hazard. Mater.*, 2020, **389**, 122075.
29 B. Zhang, A. Gleadall, P. Belton, T. McDonagh, R. Bibb and S. Qi, *Addit. Manuf.*, 2021, **46**, 102196.
30 Y. Lin and R.-Y. Tsay, *Pharmaceutics*, 2020, **12**, 582.
31 W. C. Campbell, *N. Z. Vet. J.*, 1981, **29**, 174–178.
32 Z. Adamczyk, M. Zaucha and M. Zembala, *Langmuir*, 2010, **26**, 9368–9377.
33 R. P. Pandey, K. Rasool, P. A. Rasheed, T. Gomez, M. Pasha, S. A. Mansour, O.-S. Lee and K. A. Mahmoud, *Green Chem.*, 2020, **22**, 678–687.
34 N. Minh-Hiep, I.-C. Hwang and H.-J. Park, *J. Photochem. Photobiol., B*, 2013, **125**, 194–201.
35 G. Huang, G. Qian, Y. Yan, D. Xu, C. Xu, L. Fu and B. Lin, *React. Funct. Polym.*, 2020, **146**, 104429.
36 A. A. Antipov, G. B. Sukhorukov, E. Donath and H. Mohwald, *J. Phys. Chem. B*, 2001, **105**, 2281–2284.
37 X. P. Qiu, S. Leporatti, E. Donath and H. Mohwald, *Langmuir*, 2001, **17**, 5375–5380.
38 A. Tamayo, M. A. Mazo, M. D. Veiga, R. Ruiz-Caro, F. Notario-Perez and J. Rubio, *Mater. Sci. Eng., C*, 2017, **75**, 1097–1105.
39 G. Lin, X. Chen, H. Zhou, X. Zhou, H. Xu and H. Chen, *J. Appl. Polym. Sci.*, 2019, **136**, 47160.
40 L. Ruan, M. Su, X. Qin, Q. Ruan, W. Lang, M. Wu, Y. Chen and Q. Lv, *Mater. Today Bio*, 2022, **16**, 100394.
41 E. Subbotina, T. Rukkijakan, M. D. Marquez-Medina, X. Yu, M. Johnsson and J. S. M. Samec, *Nat. Chem.*, 2021, **13**, 1118–1125.
42 P. Zimet, A. W. Mombru, D. Mombru, A. Castro, J. Pablo Villanueva, H. Pardo and C. Rufo, *Carbohydr. Polym.*, 2019, **219**, 334–343.
43 T. Li, S. Lu, J. Yan, X. Bai, C. Gao and M. Liu, *ACS Appl. Mater. Interfaces*, 2019, **11**, 10941–10950.
44 J. Chen, J. Qi, J. He, Y. Yan, F. Jiang, Z. Wang and Y. Zhang, *ACS Appl. Mater. Interfaces*, 2022, **14**, 12748–12757.
45 D. Zhang, R. Wang, C. Ren, Y. Wang, B. Li, W. Mu, F. Liu and Y. Hou, *ACS Appl. Mater. Interfaces*, 2022, 41337–41347, DOI: **10.1021/acsami.2c10899**.
46 L. Hao, L. Gong, L. Chen, M. Guan, H. Zhou, S. Qiu, H. Wen, H. Chen, X. Zhou and M. Akbulut, *Chem. Eng. J.*, 2020, **396**, 125233.